proton exchange or if it can undergo proton exchange without dissociation, we monitored the signal at mass 48 (dashed line). This mass corresponds to $DCOOD^+$ from DCOOD monomer and to $(DCOOH)H^+$ from doubly proton-exchanged dimer. The fast arrival times in the mass-48 spectrum indicate that the signal arises mostly from contaminant DCOOD monomer in the incident beam scattering inelastically from the acid, and not from $(DCOOD)_2$ reactions with the acid leading to thermally desorbing DCOOD or $(DCOOH)_2$. The three spectra demonstrate that only directly scattered dimers survive intact, whereas trapped dimers undergo both dissociation and proton exchange before the monomers desorb from the acid.

These experiments reveal that reactions with H_2SO_4 nearly always accompany the thermal accommodation of formic acid monomers and dimers on the surface of sulfuric acid. We expect chemical reactions to follow trapping if H_2SO_4 molecules within the collision zone can reorient rapidly enough to hydrogen bond to the formic acid monomer or dimer before thermal motions propel the molecules back into the gas phase (*16*). Subsequent proton transfer would then occur either within an interface that is a few molecules thick or be delayed until the formic acid molecules diffuse deeper into the acid. The observation of proton exchange in collisions between formic acid molecules and sulfuric acid implies that solvation and protonation may often be intermediate steps in the trapping and desorption of protic gas species.

REFERENCES AND NOTES

1. S. K. Chaudhuri and M. M. Sharma, *Ind. Eng. Chem. Res.* **30**, 339 (1991); D. R. Hanson and E. R. Lovejoy, *Science* **267**, 1326 (1995).
2. J. E. Hurst *et al.*, *Phys. Rev. Lett.* **43**, 1175 (1979); C. T. Rettner, E. K. Schweizer, C. B. Mullins, *J. Chem. Phys.* **90**, 3800 (1989); M. E. Saecker and G. M. Nathanson, *ibid.* **99**, 7056 (1993).
3. S. T. Govoni and G. M. Nathanson, *J. Am. Chem. Soc.* **116**, 779 (1994).
4. See also J. H. Hu *et al*, *J. Phys. Chem.* **99**, 8768 (1995); E. D. Guldan, L. R. Schindler, J. T. Roberts, *ibid.*, p. 16059; K. B. Eisenthal, *Acc. Chem. Res.* **26**, 636 (1993).
5. M. Eigen, *Angew. Chem. Int. Ed. Engl.* **3**, 1 (1964); K. Ando and J. T. Hynes, *J. Mol. Liq.* **64**, 25 (1995); and references therein.
6. The basicity of formic acid, as gauged by the acid dissociation constant K of the protonated base, is $K(\text{formic acid}\cdot H^+) \approx 10^{8.7}$. Formic acid is much less basic than water because $K(H_2O\cdot H^+) = 10^0$. See M. Liler, *Reaction Mechanisms in Sulfuric Acid* (Academic Press, New York, 1971), p. 256.
7. Uptake measurements indicate that roughly 60% of the impinging formic acid molecules dissolve in and remain within the acid during the 0.05-s observation time of the surface (K. M. Fiehrer and G. M. Nathanson, in preparation).
8. R. A. Cox, *J. Am. Chem. Soc.* **96**, 1059 (1974).
9. S. A. Lednovich and J. B. Fenn, *AIChE J.* **23**, 454 (1977).
10. Some formic acid molecules in solution may decompose into CO + H_2O. We could detect only a very noisy signal for CO desorption, in part because of a large background at the CO^+ mass due to residual N_2. See K. W. Smith, R. M. Noyes, P. G. Bowers, *J. Phys. Chem.* **87**, 1514 (1983).
11. We expect that proton exchange of DCOOD leads to DCOOH and not HCOOD. A search for double proton exchange revealed no evidence of desorbing HCOOH at mass 46 after correction for signal from desorbing DCOOH and DCOOD dissociatively ionizing into $DCOO^+$.
12. The lower limit of 3:1 is imposed by the noise in the DCOOD spectrum. The ratio of the TD intensities at a 45° exit angle should reflect the angle-integrated TD ratio because the TD channels typically follow nearly identical, cosine-like angular distributions.
13. J. Chao and B. J. Zwolinski, *J. Phys. Chem. Ref. Data* **7**, 363 (1978).
14. Enhanced nonpairwise, cooperative effects are expected to increase the basicity of the dimer over the monomer. R. Zhang and C. Lifshitz, *J. Phys. Chem.* **100**, 960 (1996); A. E. Reed, L. A. Curtiss, F. Weinhold, *Chem. Rev.* **88**, 899 (1988).
15. At lower impact energies, the monomer ion/dimer ion ratio increases as more dimers become trapped and dissociate into monomers.
16. I. Benjamin, M. A. Wilson, A. Pohorille, G. M. Nathanson, *Chem. Phys. Lett.* **243**, 222 (1995).

17. We thank F. Weinhold for discussions concerning hydrogen bonding and K. Fiehrer for the formic acid uptake measurement. This work was supported by NSF (CHE-9417909) and Presidential Young Investigator and Dreyfus Teacher-Scholar Awards to G.M.N.

18 March 1996; accepted 20 May 1996

The Morphogenesis of Bands and Zonal Winds in the Atmospheres on the Giant Outer Planets

James Y-K. Cho and Lorenzo M. Polvani

The atmospheres of Jupiter, Saturn, Uranus, and Neptune were modeled as shallow layers of turbulent fluid overlying a smooth, spherical interior. With only the observed values of radius, rotation rate, average wind velocity, and mean layer thickness as model parameters, bands and jets spontaneously emerged from random initial conditions. The number, width, and amplitude of the jets, as well as the dominance of anticyclonic vortices, are in good agreement with observations for all four planets.

Despite vast differences in chemical composition, thermodynamic properties, physical size, rotation rate, and orientation, the atmospheres of the four Jovian planets exhibit a remarkable similarity in their banded appearance and the associated strong zonal (east-west) winds. This unexpected similarity is at present a major unanswered question (*1*, *2*). Here we address this question with a single unifying dynamical framework to determine how many of the observed large-scale features of the Jovian atmospheres can be captured by a very simple physical model.

We assumed that the Jovian atmospheres can be modeled with a nearly inviscid, hydrostatically balanced, thin layer of turbulent fluid under the influence of gravitational and Coriolis forces. The motion of such a fluid (*3*) is governed by the shallow-water equations

$$\frac{\partial \mathbf{v}}{\partial t} + \mathbf{v}\cdot\nabla\mathbf{v} + f\mathbf{k}\times\mathbf{v} = -g\nabla h \qquad (1)$$

$$\frac{\partial h}{\partial t} + \nabla\cdot(h\mathbf{v}) = 0 \qquad (2)$$

where $\mathbf{v}$ is the horizontal velocity, t is time, h is the height of the fluid, $f = 2\Omega\sin\varphi$ is the Coriolis parameter, g is the gravitational acceleration, Ω is the rotation rate of the planet, φ is the latitude, and $\mathbf{k}$ is the unit vector normal to the surface of the sphere. For all four planets, h is taken starting from just below the visible cloud decks at an approximately 1000-mbar level; this is the level at which the planetary radius is commonly measured. Equations 1 and 2 were solved in spherical geometry with the use of a high-resolution, pseudospectral, parallel code (*4*). Similar equations have been used to model latitudinally confined features, principally Jupiter's Great Red Spot, in annular and channel geometries (*5*). In contrast, we extend the shallow-water model to comprise the entire planetary surface and apply it to all four planets.

The computations presented here are initialized with a random turbulent flow. The initial vorticity of this flow (Fig. 1A) is the same for all four planets, and the results are insensitive to the scale of the initial vorticity structures, provided it is chosen to be small. These computations, performed at a grid resolution of 0.7°, are essentially inviscid since more than 97% of the initial energy is conserved throughout the evolution.

The advantage of using this simple model is that only five parameters need to be specified (Table 1): Ω, g, the planetary radius a, the characteristic velocity scale U, and the mean height of the fluid layer H. The overall amplitude of the initial energy spectrum is controlled by U; the Rhines scale (*6*) L_β is

Program in Applied Mathematics and Department of Applied Physics, Columbia University, New York, NY 10027, USA.

set by U, a, and Ω; and the deformation radius L_D is determined by g, H, and Ω (7). Using for each planet the parameters in Table 1, we numerically integrated the equations starting from the initial condition shown in Fig. 1A for 300 planetary rotations, well beyond the time when a stationary state was reached in all cases.

Latitudinal bands spontaneously self-organized for all four of the planets without the use of any kind of forcing. Studies in restricted (8) and nonspherical (9) geometries have used forcing to obtain and sustain bands, and the only unforced study in spherical geometry (10) did not obtain bands because of the infinite L_D in that model (4).

The formation of a globally banded pattern from random initial conditions is apparent in the potential vorticity field (11) after only 20 planetary rotations for the Jupiter parameters (Fig. 1B). Robust zonal bands persist for long times (Fig. 1C), long after the flow pattern has become stationary. Several large, coherent vortices are spontaneously produced and persist embedded in the bands, a feature not produced in previous studies.

For Neptune as well, zonal structures appear early and eventually become stationary (Fig. 1D), but the large-scale pattern is different from that in Fig. 1C. Only three bands appear in the case of Neptune: The main one is very broad and centered around the equator, implying that over a large fraction of the spherical surface, the potential vorticity is well homogenized. This homogenization has previously been assumed (12) whereas here it is shown to be a natural end state of the turbulent shallow-water dynamics. The striking difference between Figs. 1C and 1D is a direct consequence of the fact that the ratio L_β/a is much greater for Neptune than it is for Jupiter. The ratio L_β/a is at least five times as large as L_D/a for both planets; this shows that L_β/a, and not L_D/a, controls the number of bands (4), which is roughly $\pi a/L_\beta$.

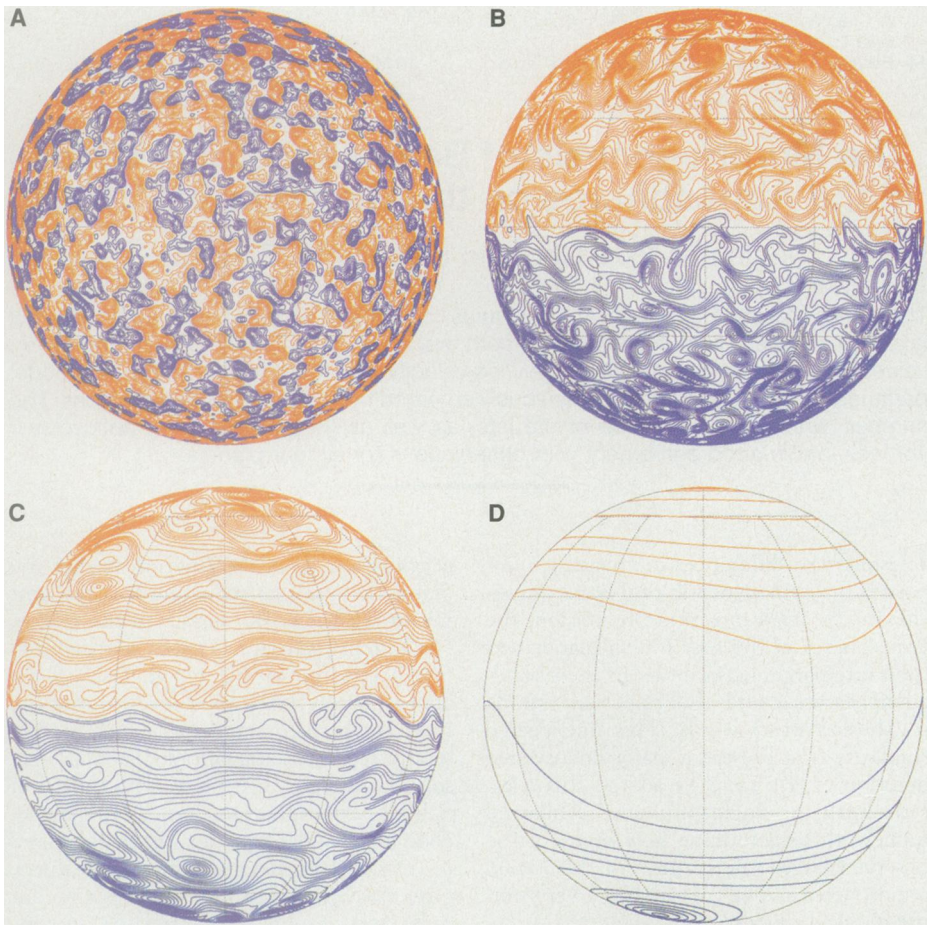

Fig. 1. (**A**) The initial vorticity, $\zeta \equiv \mathbf{k}\cdot\nabla\times\mathbf{v}$, used in our computations for all four planets (Table 1). (**B**) The potential vorticity q after 20 planetary rotations for Jupiter parameters. (**C**) Potential vorticity q after 240 planetary rotations for Jupiter parameters. (**D**) Potential vorticity q after 240 planetary rotations for Neptune parameters. Red indicates positive values, and blue indicates negative values.

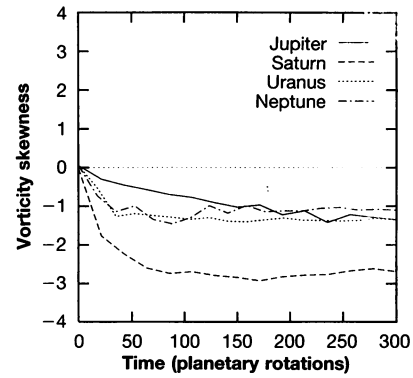

Fig. 3. The skewness of the vorticity ζ as a function of time. The initially zero value becomes negative for all four planets, showing the dominance of anticyclonic vortices.

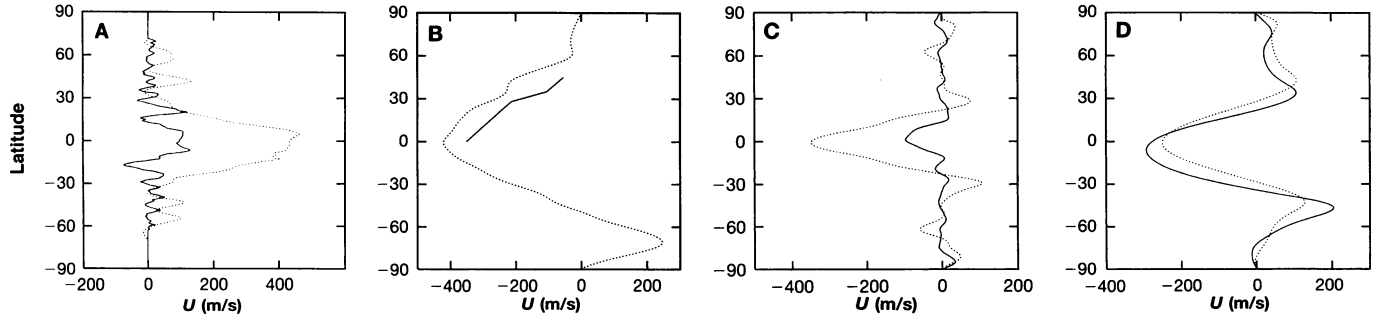

Fig. 2. The observed zonal wind profiles of (**A**) Jupiter (solid) and Saturn (dashed) and (**B**) Uranus (solid) and Neptune (dashed) from (15). The corresponding profiles for (**C**) Jupiter (solid) and Saturn (dashed) and (**D**) Uranus (solid) and Neptune (dashed) from our computations after 300 planetary rotations.

Table 1. Physical parameters used in our model. Values from (*1, 15*).

Planet	a (10^7 m)	$2\pi/\Omega$ (hours)	g (m/s^2)	U (m/s)	H (10^3 m)
Jupiter	7.1	9.9	23	50	20
Saturn	6.0	10.7	9	300	40
Uranus	2.6	−17.2	9	300	35
Neptune	2.5	17.9	11	300	30

Alternating potential vorticity gradients (Fig. 1) indicate the presence of strong zonal jets, as in the observations: Jupiter and Saturn have multiple jets and a prograde (eastward) equatorial wind (Fig. 2A), whereas Uranus and Neptune have large retrograde (westward) equatorial winds (Fig. 2B). Our shallow-water computations (Fig. 2, C and D) capture the approximate number, width, and amplitude of the observed zonal winds for all four planets. Precise, quantitative agreement is neither sought nor expected, given the simplicity of this model. The important point is that the values in Table 1 alone are sufficient to determine the gross features of the zonal winds. One feature that the model seems unable to reproduce is the direction of the equatorial jets for Jupiter and Saturn, indicating that a more sophisticated model is necessary for those two planets. Furthermore, our model predicts that more anticyclones than cyclones (*13*) are to be found on all four planets. This asymmetry is depicted by the skewness of the vorticity field (Fig. 3). The negative bias is observationally well established for Jupiter (*14*) but is not as robustly determined for the other planets.

In conclusion, our study strongly suggests that, however different the Jovian planets may be, their characteristic banded appearance is a direct consequence of the intrinsic shallow-water dynamics they all share.

REFERENCES AND NOTES

1. A. P. Ingersoll, *Science* **248**, 308 (1990).
2. P. J. Gierasch, *J. Geophys. Res.* **98**, 5459 (1993).
3. P. S. Laplace, *Mem. l'Acad. R. Sci. Paris* **88**, 75 (1775); H. Lamb, *Hydrodynamics*, (Dover, New York, 1932); J. Pedlosky, *Geophysical Fluid Dynamics* (Springer-Verlag, New York, 1979).
4. J. Y-K. Cho and L. M. Polvani, *Phys. Fluids* **8**, 1531 (1996).
5. P. S. Marcus, *Nature* **331**, 693 (1988); T. E. Dowling and A. P. Ingersoll, *J. Atmos. Sci.* **46**, 3256 (1989).
6. P. B. Rhines, *J. Fluid Mech.* **69**, 417 (1975).
7. The values of $L_D \equiv \sqrt{gH}/2\Omega$ are the least reliable of the parameters in Table 1, because of the poor knowledge of the vertical structure of the atmospheres of these planets. However, the number of bands in our computations is insensitive to the precise value of L_D; the number is controlled by $L_\beta \equiv \sqrt{Ua}/\Omega$.
8. G. P. Williams, *J. Atmos. Sci.* **35**, 1399 (1978).
9. M. E. Maltrud and G. K. Vallis, *J. Fluid Mech.* **228**, 321 (1991).
10. S. Yoden and M. Yamada, *J. Atmos. Sci.* **50**, 631 (1993).
11. The potential vorticity $q \equiv (\zeta + f)/h$ is conserved following the motion of each fluid element, thus serving as a tracer for the flow, and is the dynamically significant quantity to view. See, for instance, B. J. Hoskins, M. E. McIntyre, A. W. Robertson, *Q. J. R. Meteorol. Soc.* **111**, 877 (1985).
12. B. A. Smith *et al.*, *Science* **246**, 1422 (1989); L. M. Polvani, J. Wisdom, E. DeJong, A. P. Ingersoll, *ibid.* **249**, 1393 (1990); M. Allison and J. T. Lumetta, *Geophys. Res. Lett.* **17**, 2269 (1990).
13. Anticyclones are eddies with negative vorticity in the northern hemisphere and positive vorticity in the southern hemisphere. Cyclones are the converse.
14. M.-M. McLow and A. P. Ingersoll, *Icarus* **65**, 353 (1986).
15. R. Beebe, *Chaos* **4**, 113 (1994).

16. This work is supported by NSF. The computations were performed on the Cray C90 at the Pittsburgh Supercomputing Center. We are grateful to M. Allison for thoughtful suggestions on the manuscript and to A. Simon and R. Beebe for the zonal wind data in Fig. 2.

26 March 1996; accepted 3 June 1996

A Magnetic Signature at Io: Initial Report from the Galileo Magnetometer

M. G. Kivelson, K. K. Khurana, R. J. Walker, C. T. Russell, J. A. Linker, D. J. Southwood, C. Polanskey

During the inbound pass of the Galileo spacecraft, the magnetometer acquired 1 minute averaged measurements of the magnetic field along the trajectory as the spacecraft flew by Io. A field decrease, of nearly 40 percent of the background jovian field at closest approach to Io, was recorded. Plasma sources alone appear incapable of generating perturbations as large as those observed and an induced source for the observed moment implies an amount of free iron in the mantle much greater than expected. On the other hand, an intrinsic magnetic field of amplitude consistent with dynamo action at Io would explain the observations. It seems plausible that Io, like Earth and Mercury, is a magnetized solid planet.

Jupiter's moon Io has repeatedly surprised planetary scientists. First, Io's orbital position was unexpectedly found to control decametric radio emission from Jupiter's ionosphere (*1*). Early explanations suggested that the emissions were generated by magnetic field–aligned currents linking Io and Jupiter (*2*). These ideas were refined and linked to Alfvénic disturbances generated by the interaction of the flowing plasma of Jupiter's magnetosphere with an electrically conducting Io (*3, 4*). After the discoveries of a large cloud of neutral sodium surrounding Io (*5*) and of a torus of ionized sulfur encircling Jupiter at the distance of Io's orbit (*6*), Voyager 1 found volcanic plumes distributed on the surface of the moon (*7*). The Voyager 1 magnetometer detected magnetic perturbations of ~5% of the ambient jovian magnetic field (~1900 nT) as it crossed Io's magnetic flux tube about 11 R_{Io} (radius of Io, 1821 km) below Io (*8*), thereby confirming the presence of a field-aligned current flowing several thousand kilometers away from the spacecraft and carrying more than 10^6 A into the jovian ionosphere.

M. G. Kivelson, K. K. Khurana, R. J. Walker, C. T. Russell, Institute of Geophysics and Planetary Physics, University of California, Los Angeles, Los Angeles, CA 90095–1567, USA.
J. A. Linker, Science Applications International Corporation, San Diego, CA 92171, USA.
D. J. Southwood, Department of Physics, Imperial College of Science, Technology, and Medicine, London, SW7 2BZ, UK.
C. Polanskey, Jet Propulsion Laboratory, Pasadena, CA 91109, USA.

The Galileo spacecraft flew by Io on 7 December 1995; its closest approach was at 17:45:58 UT (universal time) at an altitude of 898 km (*9*). Particles and fields data from the pass recorded on the spacecraft tape recorder will be analyzed in the early summer of 1996. However, survey data (*10*) read out directly from the magnetometer's (*11*) internal memory were returned in late December 1995. All three components of the background jovian field measured on Galileo's trajectory through the plasma torus followed predictions based on a recent extension (*12*) of Voyager-epoch magnetic field models (*13*) but in the wake of Io (that is downstream in the flow of torus plasma corotating with Jupiter), the field magnitude decreased by 695 nT in a background of 1835 nT (Fig. 1). Perturbations of the field along the spacecraft's trajectory were principally antiparallel to the model jovian field (Fig. 2). The field rotated slightly, but the bending was not what would be produced if the field had been pushed outward around Io but rather that caused by a field pulled inward toward Io. Indeed, the perturbations along the spacecraft trajectory are quite well represented by a model in which Jupiter's field is merely added to the field of an Io-centered dipole with moment aligned with the local field of Jupiter (hence antiparallel to Jupiter's dipole moment) (Fig. 3).

As the local corotation speed is greater than the Keplerian speed, the jovian plas-